OPTIMIZING THE HEAT TREATMENT OF HIGH-STRENGTH 7075-TYPE WROUGHT ALLOYS: A METALLOGRAPHIC STUDY

Mohamed F. Ibrahim, Guillermo H. Garza-Elizondo, Agnes M. Samuel, and Fawzy H. Samuel
Université du Québec à Chicoutimi, Chicoutimi, QC, Canada

DOI 10.1007/s40962-016-0038-2

Abstract

The main objective of this study was to optimize the 7075 alloy strength. Several experimental alloys were prepared and tensile test bars were cast, using an ASTM B-108 type permanent metallic mold. The as-cast samples were then solution heat-treated at 470 °C (878 °F) for times up to 48 h. The solution heat-treated bars were also aged in order to improve the alloy strength through precipitation hardening. The newly developed versions of the 7075 alloy displayed an ultimate tensile strength of ~1 GPa. A detailed study of phase precipitation in these alloys using electron probe microanalysis; energy-dispersive spectroscopy; and wavelength-dispersive spectroscopy analysis techniques showed that the marked increase in alloy strength may be attributed to precipitation of dense ultrafine particles of Al_2Cu phase distributed uniformly throughout the matrix. Fracture mechanisms of the alloys at different heat treatment conditions were also investigated. With the use of proper additives, cold/hot deformation, homogenization and aging, 7075 alloys have the potential to reach very high ultimate tensile strength levels after aging (compared to 580 MPa obtained from traditional 7075 alloy).

Keywords: *7075-type alloys, microstructural characterization, high-strength alloys, alloy development, precipitation hardening*

Introduction

Many studies[1–8] have been reported on the effect of heat treatment of 7075 alloys. The solution treatment and aging temperatures are the main factors controlling the relative precipitation of alloying elements in the grain boundaries, with solution temperature having the main influence on grain boundary segregation. The precipitates at the grain boundaries were found to consist of large amounts of Mg, Si and Al along with lesser amounts of Zn and Cu. The Zn-rich precipitates were predominant in heat treatments during low solution temperature annealing at 394 °C (741 °F), while the Fe-rich precipitates were predominant at high solution temperatures [482–527 °C (900–981 °F)].[8] Precipitates with high interfacial energies tend to precipitate at grain boundaries, resulting in embrittlement. Low interfacial energy means easy nucleation, a uniform precipitate distribution and resistance to coarsening at elevated temperatures.[9]

The microstructure of commercial 7075 alloy in the peak-aged (T651) temper predominantly contains the $\acute{\eta}$ transition phase before formation of the stable η-$MgZn_2$ phase. Some of these transition phase particles are heterogeneously nucleated on dislocation lines. In the T7 microstructure, the overall particle concentration is high, consisting mainly of coarse transition phase particles $\eta 1$, $\eta 2$ and $\eta 4$ besides a small amount of fine particles of the last three phases. Increases in the hardness of the 7075 alloy are believed to arise mainly from the fine dispersion of small $\acute{\eta}$ particles.[10] Retrogression and re-aging (RRA) treatments for 7075 alloy sheets at various temperatures [180, 200 and 220 °C (356, 392 and 428 °F)] and times (2–80 min) showed that an increase in treatment temperature decreased both the hardness and strength, while increasing the impact toughness. This can be explained by the dissolution of phases in the matrix during RRA and enlargement of segregation during subsequent aging. The decrease in the hardness in the first stage of RRA is explained by the partial dissolution of the Guinier–Preston (GP) zones, while the subsequent increase in hardness refers to the formation and growth of the $\acute{\eta}$-phase to a specific size of stable η particles.[11]

A version of this paper was previously published in 2015 AFS Transactions.

The microstructure of the grain boundary particles, which depends on the aging process, is the main parameter controlling the 7075 alloy mechanical properties. The high strength of this alloy in the RRA temper is considered to arise from both the presence of many fine η particles, which are probably coherent, and of the high overall concentration of particles in this structure.[12] The double aging (DA) of 7075 alloy has positive effect on hardness, yield and ultimate tensile strengths. Moreover, double aging to peak hardness results in a significantly reduced processing time from 48 to 2 h, which can lead to reduced energy and cost. Thermomechanical double aging (TDA) causes further acceleration of precipitation, reducing the total heat treatment time to 80 min, with an increase in both hardness and strength, but a decrease in the ductility relative to single aging.[13] During a study of secondary aging, it was concluded that the T614 temper produces tensile properties close to or greater than those for the T6 condition; the fracture toughness is enhanced as well. The T814 and T914 tempers are effective in utilizing secondary precipitation, while the T816 and T916 produce improved mechanical properties.[14]

Farhadi et al.[15–17] carried out a detailed study on the effects of small additions of Be and Sr on the microstructure and tensile properties of experimental 6xxx alloys. Their results showed that for 0.02 %Be addition, the iron intermetallics precipitate in the form of small, globular α-Al_8Fe_2SiBe particles in the interdendritic regions. Combined addition of Be and Sr leads to the precipitation of α-Al_8Fe_2SiBe phase as very fine, broken particles, which markedly enhances the alloy formability. The authors also found that the addition of 0.02 %Be reduces the possibility of hot tearing during solidification and protects the outer surfaces of the cast test bars from oxidation during solution heat treatment at high temperatures.

In a previous work, the present authors briefly described the methods of obtaining super-strong 7075-based alloy using experimental and industrial alloys.[18] The main objective of the study presented here was to understand the hardening mechanism for achieving ultimate tensile strength of $\sim$1 GPa as compared to 580 MPa obtained from the current alloys following aging at 120 °C (248 °F) for 24 h through adjusting the alloy composition and heat treatment technique of the 7075-type alloys.

Experimental Procedures

Experimental 7075 alloy was prepared through the addition of measured amounts of Mg, Zn, Si, Cu and Fe to the melt of commercially pure aluminum. Alloying elements were added in the form of master alloys or pure metals to obtain the predetermined level/levels of each element. Table 1 shows the average chemical composition of the commercial pure aluminum and the base alloy investigated. In

Table 1. Chemical Composition (wt%) of the Base Metal, Base Alloy and New Alloy

Alloy code/alloying elements	Si	Fe	Cu	Mn	Cr	Ni	Zn	Mg	Ti	Zr	Be
Pure aluminum	0.050	0.090	<0.001	<0.001	<0.001	0.006	0.002	<0.001	0.005	<0.001	<0.001
A (base alloy)	0.172	0.384	1.980	0.330	0.303	0.022	6.420	2.260	0.016	0.211	<0.001
New alloy	0.10–0.40	0.12–0.50	1.20–2.00	0.06–0.30	0.2–0.40	0.05–0.40	5.20–6.50	1.5–3.0	0.06–0.20	0.1–0.35	0.001–0.10

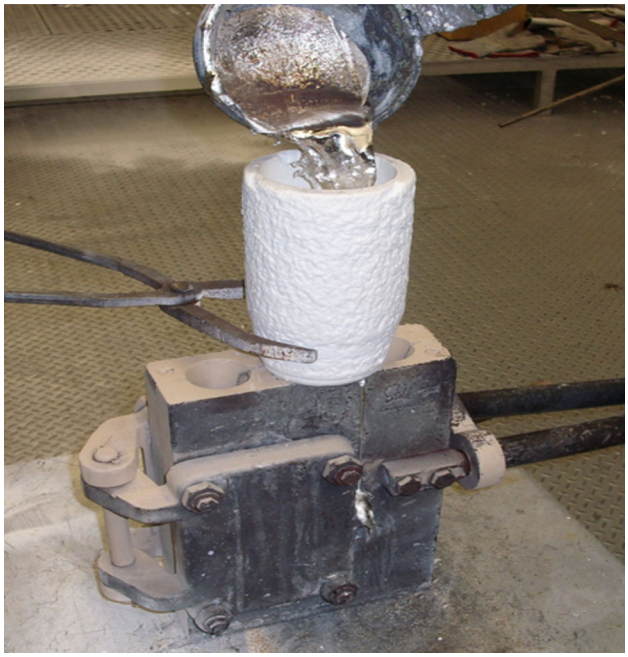

Figure 1. Casting setup used in the present work.

addition, another alloy was also developed in this study, derived from alloy A (proprietary composition). Prior to casting, the molten metal was degassed for 15 min using pure, dry argon to remove dissolved gases and inclusions. Alloy castings were produced using an ASTM: B-108 permanent mold as shown in Figure 1. At the bottom of the pouring cup, a ceramic foam filter (10 ppi) was placed to prevent inclusions and oxide films from entering the mold. In order to avoid hot tearing, small amounts of TiB_2, Zr and Be were added in the form of Al-5 %Ti-1 %B, Al-25 %Zr and Al-2 %Be master alloys, respectively.[17–19] The permanent mold was preheated at 450 °C (842 °F).

The test bars were prepared for each alloy composition and divided into different sets according to both the recommended traditional heat treatment and the proposed new heat treatment conditions. Six sets of the base alloy were conventionally heat-treated, where all of them were solution heat-treated at 470 °C (878 °F)/8 h, and then quenched in 65 °C (149 °F) warm water. One set was kept in the solution heat-treated condition, while the other five sets were subjected to different aging conditions: single aging at 120 °C (248 °F)/24 h; single aging at 280 °C (536 °F)/8 h; double aging at 120 °C (248 °F)/24 h, followed by 180 °C (356 °F)/8 h; the fourth set had retrogression and re-aging at 120 °C (248 °F)/24 h, 180 °C (356 °F)/8 h, followed by 120 °C (248 °F)/24 h and, finally, the last set was subjected to retrogression and re-aging at 120 °C (248 °F)/24 h, 280 °C (536 °F)/8 h, followed by 120 °C (248 °F)/24 h, respectively. Two sets of the new alloy were heat-treated by means of homogenization and a proposed new aging process (proprietary process). For each heat treatment, ten test bars were used.

Tensile testing was carried out for the heat-treated test bars at room temperature using an MTS servohydraulic mechanical testing machine working at a strain rate of 1.0×10^{-4} s^{-1}. The elongation of the tested specimens was measured using a strain gauge extensometer attached to the specimen during the tension test. A data acquisition system attached to the MTS machine provided the results. For each sample tested, the stress–strain curve obtained illustrated the mechanical behavior of the specimen under the loads applied. Ten tensile test bars for each composition were tested in the heat-treated conditions. For the new alloy, the test bars were tested using the same MTS tensile testing machine.

The microstructures of the polished sample surfaces were examined using a JEOL 840A electron probe microanalyzer equipped with energy dispersive X-ray spectroscopic (EDS) and WDS facilities. Precipitation taking place during the aging process was examined using an SU-8000 Field Emission Scanning Electron Microscope (FE-SEM), while the fracture surfaces of selected tensile-tested samples were examined using a Hitachi S-2700 SEM.

Table 2. Tensile Properties of 7075-Type Alloys/Conditions Studied

Alloy code and heat treatment condition	UTS (MPa)	El (%)
A/Solution heat treatment [8 h @ 470 °C (878 °F)]	429	4.63
A/Single aging [24 h @ 120 °C (248 °F)]	580	1.01
A/Single aging [8 h @ 280 °C (536 °F)]	386	4.16
A/Double aging [24 h @ 120 °C (248 °F)] + [8 h @ 180 °C (356 °F)]	525	0.92
A/Retrogression and re-aging at 120 °C (248 °F)/24 h, 180 °C (356 °F)/8 h, 120 °C (248 °F)/24 h	496	1.02
A/Retrogression and re-aging at 120 °C (248 °F)/24 h, 280 °C (536 °F)/8 h, 120 °C (248 °F)/24 h	312	3.5
New alloy/homogenization and stretching	597	3.62
New alloy/double aging [24 h @ 120 °C (248 °F)] + [8 h @ 180 °C (536 °F)]	580	1.58
New alloy/proposed new aging process	820	1.13

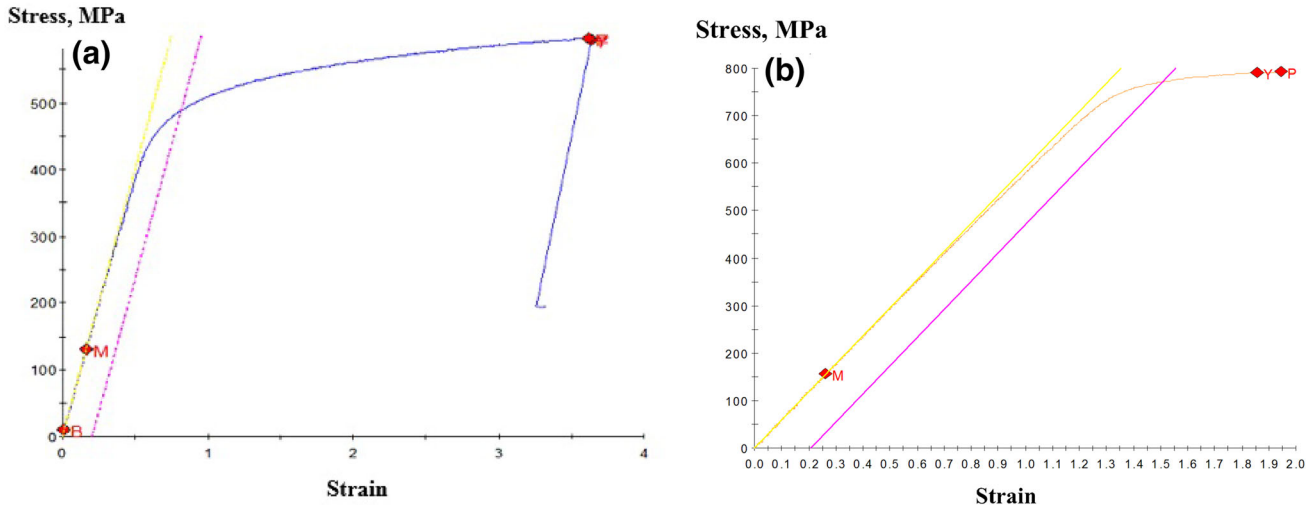

Figure 2. Stress–strain diagrams obtained from (a) base 7075 alloy (alloy A) after single aging at 120 °C (248 °F) for 24 h and (b) new alloy (alloy B) after proprietary aging treatment.

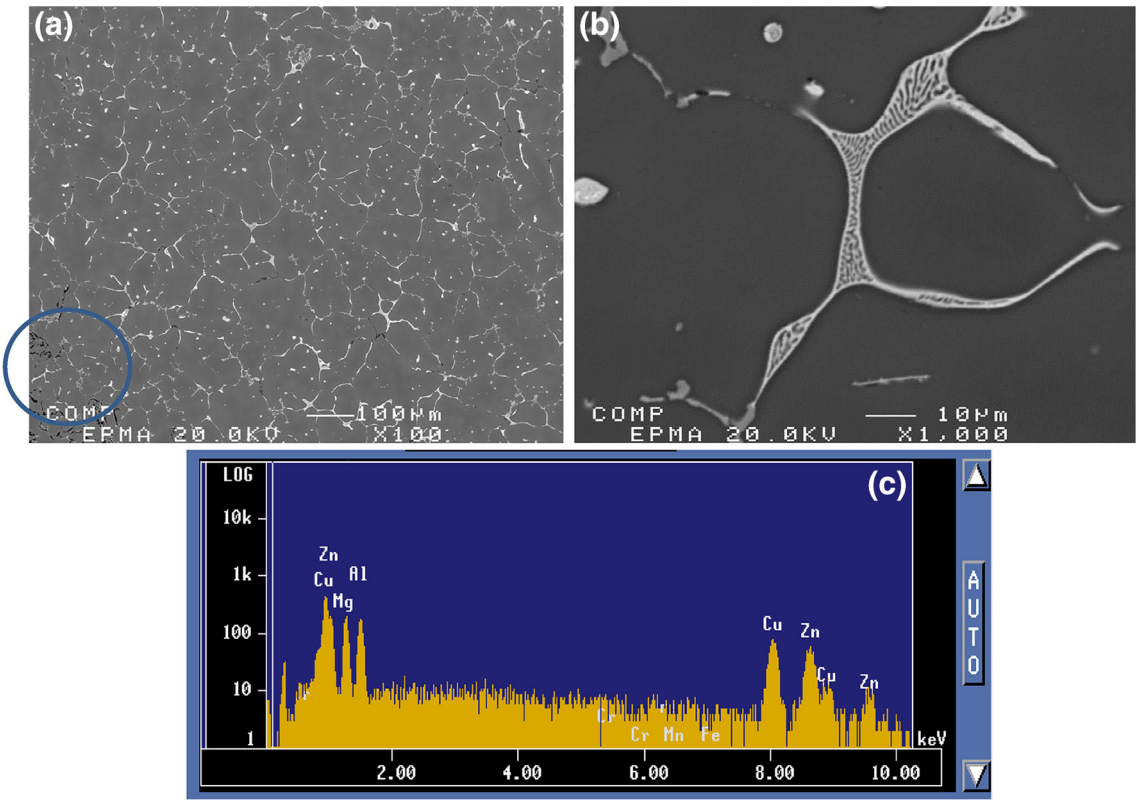

Figure 3. (a, b) Backscattered electron images revealing the microconstituents in the base alloy in the as-cast condition: (a) low magnification image illustrates the presence of fine cracks in the white circle due to shrinkage; (b) high magnification image illustrating the details of the eutectic AlMgCuZn phase—it should be noted that the spherical particles in the middle of the grain have the same structure. (c) EDS spectrum from (b), displaying strong peaks due to Al, Mg, Cu and Zn.

Results and Discussion

Tensile Properties

Several authors have studied the effects of alloying elements on the mechanical properties of 7075 alloys in addition to that of heat treatment.[19–23] The Ag-free T6-tempered [121 °C (250 °F)/24 h] 7075 alloys exhibit low strengths that are attributed to a relatively coarse dispersion of the hardening precipitates while the Ag-containing alloys show higher strengths. When Cr and Mn are added to the Ag-containing alloys, they result in low strengths as with the Ag-free alloys, due to quench sensitivity of particles containing either Cr or Mn. On the other hand, adding these two elements to Ag-free alloys resulted in higher strengths. Adding 0.3–0.4 % Ag did not increase the strength of single- and double-aged alloys in both T6 and T7 treatments [121, 157, 162 and 177 °C (250, 315, 324 and 351 °F)], whereas the stress corrosion cracking (SCC) resistance was improved. Alloys containing Cr, particularly those also containing Zr and Mn, were more resistant and increased in strength, as a result of the reduced sensitivity to quenching rate. Higher strengths were obtained by increasing the Cu content in alloy containing Mn and Zr in the case of double-aging treatments.[19,20]

Direct chill (DC) cast 7XXX series, modified with Zr and Sc, revealed the following: (1) Sc additions produced a grain-refined microstructure with an equiaxed grain morphology, where 0.18 %Sc reduced the grain size to 120 μm and inhibited the formation of twinned columnar grains and solidification cracks; (2) higher Sc levels of 0.38 % and 0.48 % formed the brittle primary $Al_3(Sc, Zr)$ phase, which led to a deterioration in the mechanical properties; (3) homogenization and T6 treatments developed both the strength and ductility of alloys containing Sc, where the yield strength obtained was 490–590 MPa along with 15 % elongation at room temperature, but at liquid nitrogen temperature [−196 to −210 °C (−321 to −346 °F)], these values were 610 MPa and 10 %, respectively, with a UTS of 720 MPa.[21] The Sc-modified 7075 alloy presented the highest strength (640 MPa) and significantly increased the SCC resistance. Adding 0.2 % Sc resulted in formation of the $Al_3(Sc_{1-x}Zr_x)$ phase which refined the microstructure. The addition of Ce had little strengthening effect.[22] The addition of 2 %Al-5Ti-1B master alloy to Al-12 Zn-3Mg-2.5Cu alloy reduced its grain size from 480 to 40 μm; the hardness of both Ti-refined and T6-tempered alloy was significantly increased.[23] In the present work, the effects of alloying elements used (Table 1), and the heat treatment conditions

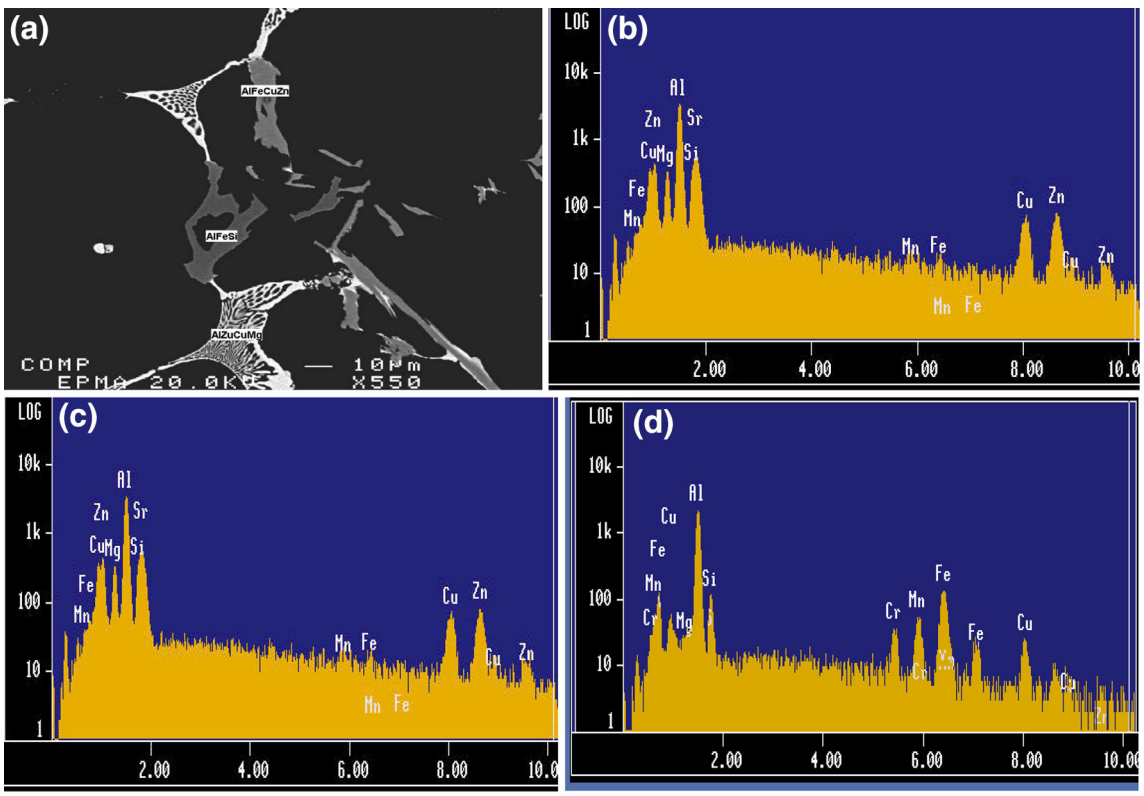

Figure 4. (a) Backscattered electron image of the as-cast microstructure of the base alloy; (b–d) EDS spectra, respectively, corresponding to the AlFeCuZn, AlFeSi and AlZnCuMg phases shown in (a).

applied (Table 2) on such alloys are brought out in terms of the tensile properties summarized in Table 2.

Figure 2 displays the stress–strain diagrams obtained from both the base 7075 alloy and the newly developed alloy under different heat treatment conditions. The maximum attainable UTS was 580 MPa for samples of the base alloy subjected to single aging at 120 °C (248 °F)/24 h, which is normally higher than that of the solution heat-treated alloy (429 MPa), while the minimum UTS reached was 312 MPa for retrogression and re-aging samples treated at 280 °C (536 °F)/8 h, followed by 120 °C (248 °F)/24 h, as a result of over-aging, dissolution of phases in the matrix during retrogression treatment, and segregation of some particles at the grain boundaries. The best aging condition was, as recommended, single aging at 120 °C (248 °F)/24 h. Compared to the base 7075 alloy in the current study, the new alloy after homogenization and stretching resulted in a UTS of 597 MPa (~600 MPa) while, after the proposed aging process, the UTS was 980 MPa (~1 GPa) which renders this alloy, following the proposed heat treatment technique, as a super-strong alloy.

Microstructural Characterization

Figure 3a, b reveals backscattered images of the base alloy as-cast microstructure taken at low (Figure 3a) and high (Figure 3b) magnifications, where the AlFeCuZn phase is seen precipitated on the grain boundaries as well as within the grains. Figure 3c shows an EDS spectrum corresponding to the AlMgCuZn phase in the as-cast structure. The high-magnification backscattered image of the as-cast microstructure of the base alloy shown in Figure 4a reveals the presence of AlFeCuZn, AlFeSi and AlZnCuMg phases as well. Figure 4b–d shows the EDS spectra corresponding to the latter three phases detected in the as-cast structure. Figure 5a shows a backscattered image of the base alloy microstructure after solution heat treatment, while the high-magnification images shown in Figure 5b, c demonstrate the presence of the α-Fe and AlFeCu insoluble phases. Figure 5d shows the EDS spectrum corresponding to the AlFeCu phase detected in the homogenized structure. Table 3 summarizes the identification of the phases observed in Figures 4 and 5, which is in good agreement with those reported in the literature.

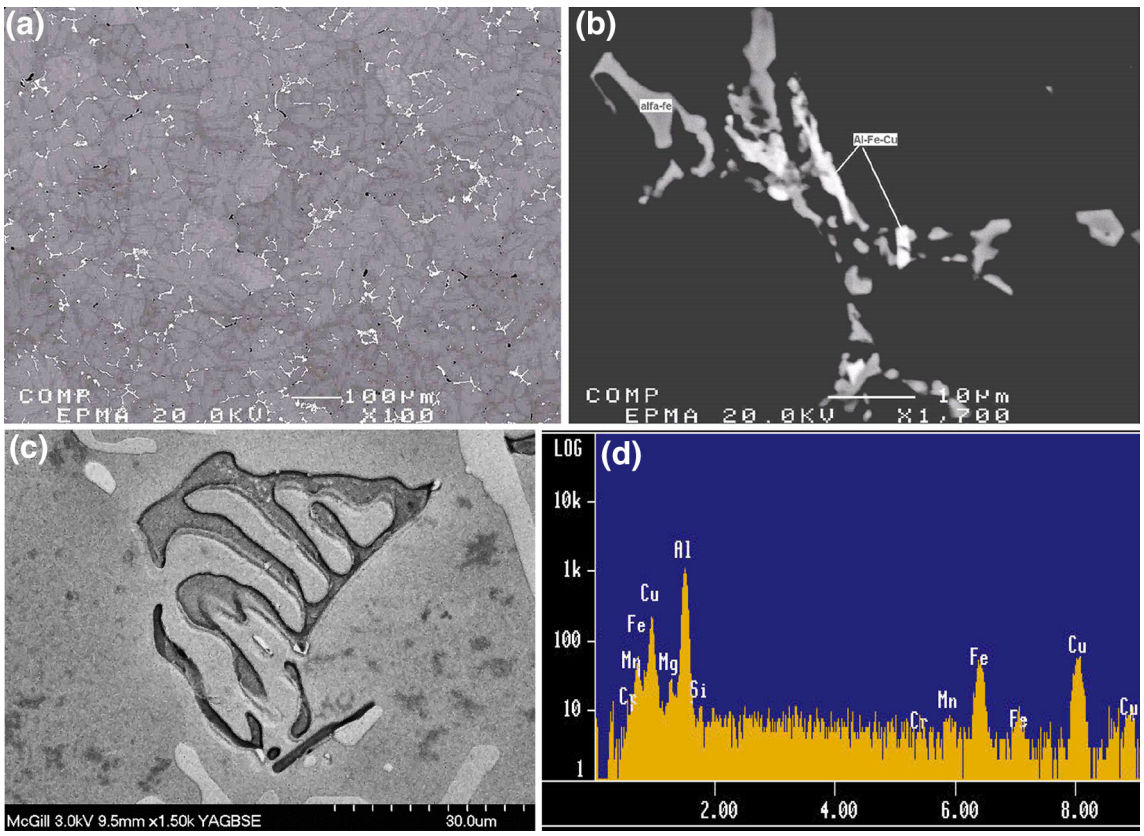

Figure 5. Backscattered electron images of (a) solution heat-treated base alloy, showing (b) presence of AlFeCu and α-Fe intermetallic phases in (a); (c) high-magnification image (b); and (d) EDS spectrum corresponding to the AlFeCu phase observed in (b).

For all microstructures studied, line scans were used to investigate the distribution of alloying elements before and after solution heat treatment for both the base and new alloys. These scans revealed the distribution of three common elements Mg, Cu and Zn in the as-cast 7075 alloys. The peaks corresponding to the Mg, Cu, and Zn concentrations in the as-cast samples disappeared after solution treatment, reflecting the optimized homogeneity of the solution-treated alloys. Conventional and/or commercial heat treatment of 7075 alloy led to maximum UTS of 580 MPa. In order to arrive at a better understanding of the precipitation sequence in the newly developed alloy, samples for SEM examination were cut from the tensile-tested bars [~10 mm (0.39 in.) away from the fracture surface]. The polished samples were examined using a Hitachi SU-8000 FE-SEM operating at 5 kV equipped with an EDS system. Figure 6a shows a backscattered electron image of an as-cast sample of the new alloy, showing a few rod-like shaped particles. These particles were identified as being mostly Al_2Cu phase from the corresponding EDS

Table 3. Identification of Phases Observed in Figures 4 and 5

Figure no.	Element (at %)								Approximate composition
	Si	Al	Fe	Cr	Cu	Mg	Mn	Zn	
4a	0.140	26.827	0.168	0.009	21.078	34.271	0.040	17.42	$T(Al_3Cu_2Mg_4Zn_2)$
5b	0.617	75.332	16.755	0.968	2.311	0.049	3.310	0.554	$Al_3(Fe,Cu,Mn,Cr)$
5b	3.683	77.508	11.006	2.485	0.717	0.079	3.918	0.578	$Al_8(Fe,Mn,Cr)_2Si/Al_{15}(Fe,Mn,Cr)_3Si_2$

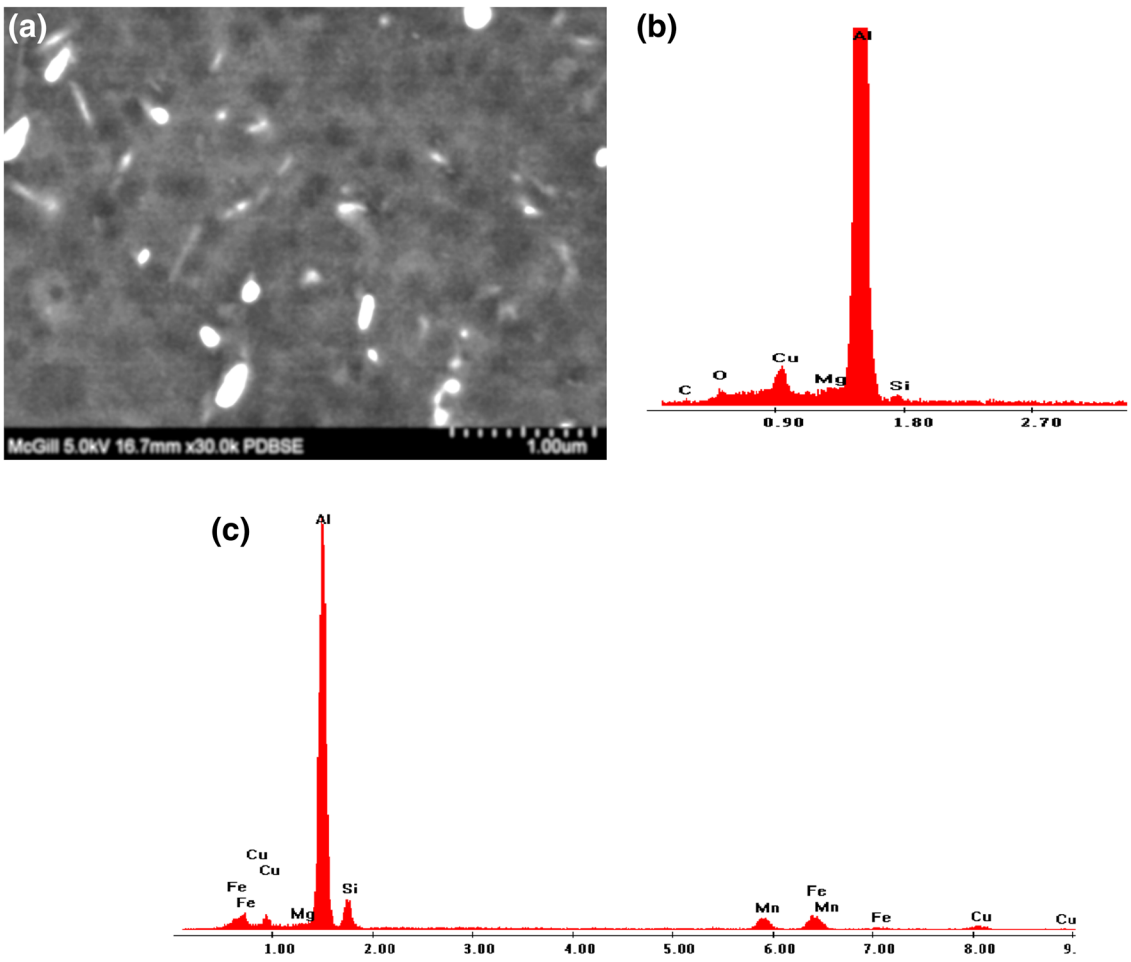

Figure 6. The following are shown: (a) backscattered electron image of the new alloy in the as-cast condition; (b) EDS spectrum corresponding to Al_2Cu phase; and (c) EDS spectrum corresponding to α-$Al_{15}(Fe,Mn)_3Si_2$ phase.

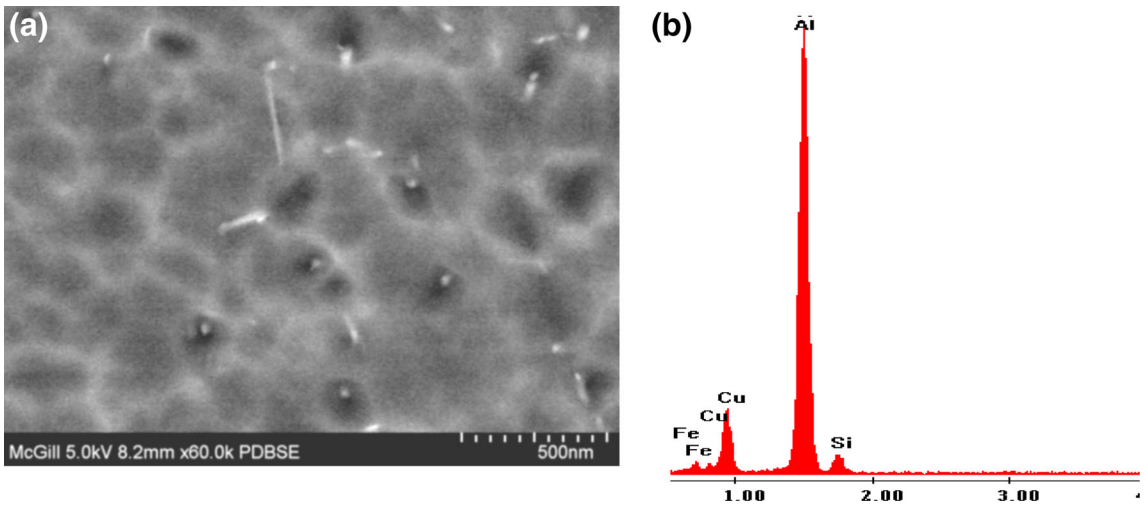

Figure 7. (a) Backscattered electron image of the new alloy after solution heat treatment and (b) EDS corresponding to (a) shows the presence of Cu and Fe peaks.

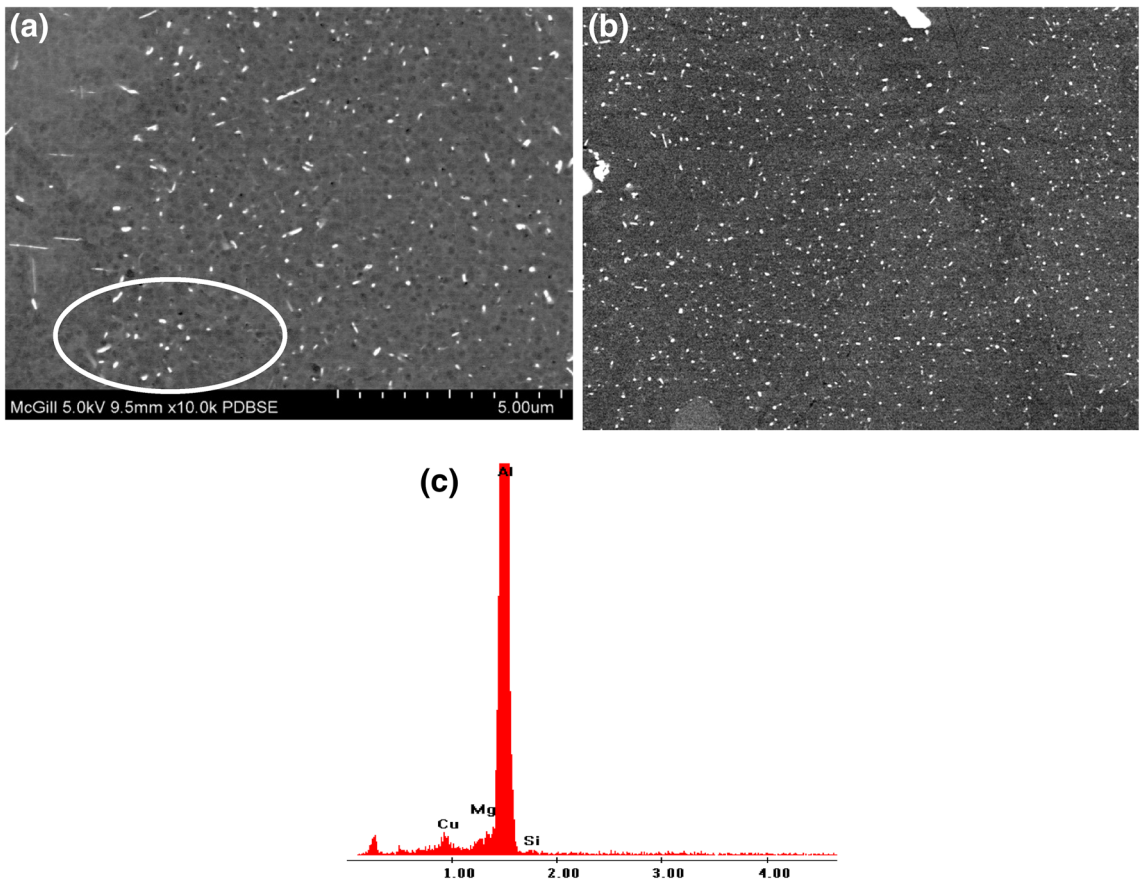

Figure 8. Backscattered electron images show precipitation in the new alloy under different conditions: (a) homogenization and stretching, (b) double aging [24 h at 120 °C (248 °F) + 8 h at 180 °C (356 °F)], and (c) EDS spectrum corresponding to (a) showing reflections mainly due to Al and Cu elements.

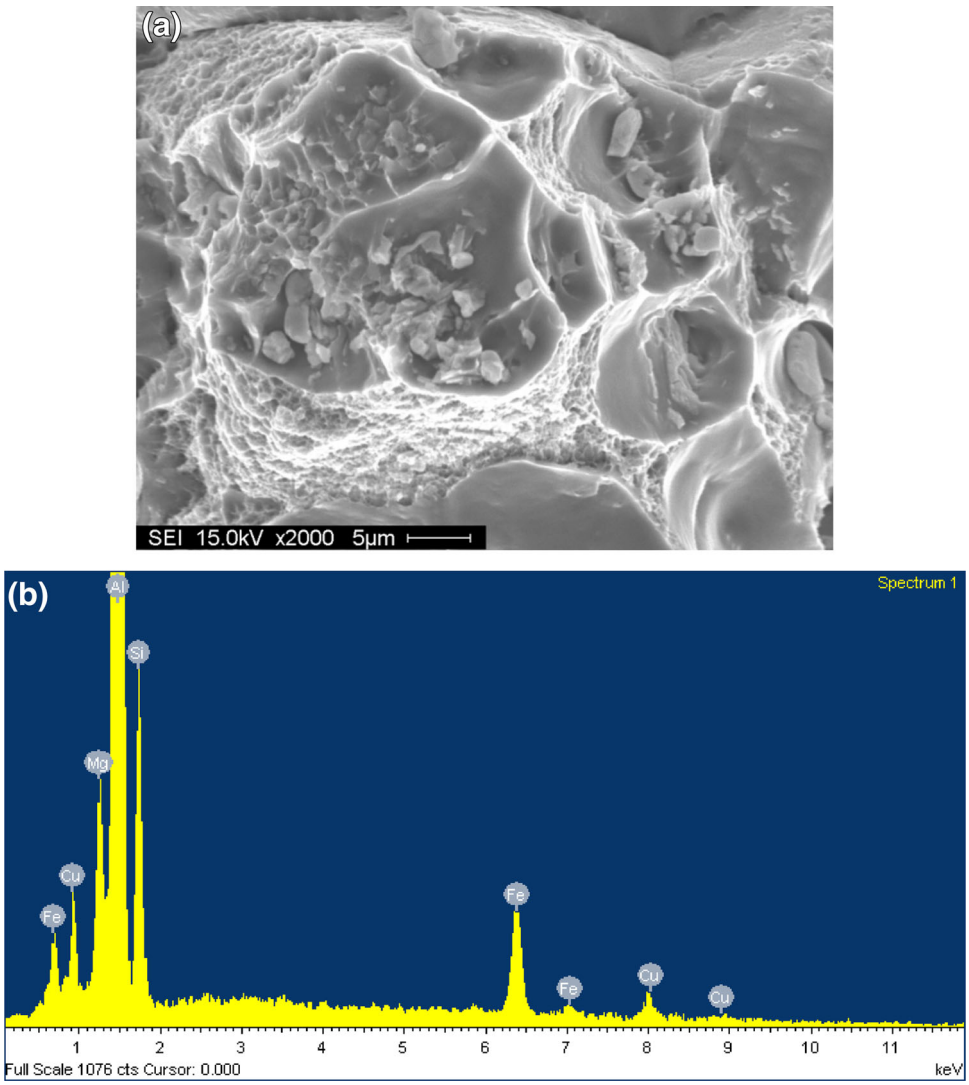

Figure 9. (a) Secondary electron image showing the fracture surface of new alloy after homogenization, and (b) EDS spectrum corresponding to the particles within the dimples in (a) revealing Al, Mg, Fe and Cu peaks.

spectrum (Figure 6b), together with some α-Fe intermetallic phase particles (Figure 6c). As can be observed from Figure 7a, most of the Al_2Cu phase particles have dissolved in the aluminum matrix after the homogenization and quenching treatment, with fragments of α-Fe phase particles still present in the matrix (Figure 7b).

Double-aging treatment of 24 h at 120 °C (248 °F) followed by 8 h at 180 °C (356 °F) resulted in intense precipitation of ultrafine particles with two distinct morphologies: spherical (encircled) and rod-like, due to their precipitation at two different temperatures (Figure 8a). Aging the new alloy using the new technique resulted in the precipitation of dense spherical particles throughout the matrix (Figure 8b). These precipitates are mainly Al_2Cu phase particles as confirmed by the associated EDS spectrum displayed in Figure 8c. These precipitates are believed to be the reason for the observed high strength achieved in the new alloy at 120 °C/24 h (248 °F/24 h), which is normally higher than the solution heat-treated alloy (429 MPa), while the minimum UTS reached was 312 MPa for retrogression and re-aging samples at 280 °C/8 h (536 °F/8 h), followed by 120 °C/24 h (248 °F/24 h) as a result of over-aging effect, dissolution of phases in the matrix during retrogression treatment, and segregation of some particles at the grain boundaries. The best aging condition was, as recommended, single aging at 120 °C/24 h (248 °F/24 h). Compared to the 7075 alloy, the base alloy in the current study, the new alloy after homogenization and stretching resulted in a UTS of 597 MPa (~600 MPa) while, after the proposed aging process, the UTS increased to 980 MPa (~1 GPa), which renders this alloy in the category of a super-strong alloy.

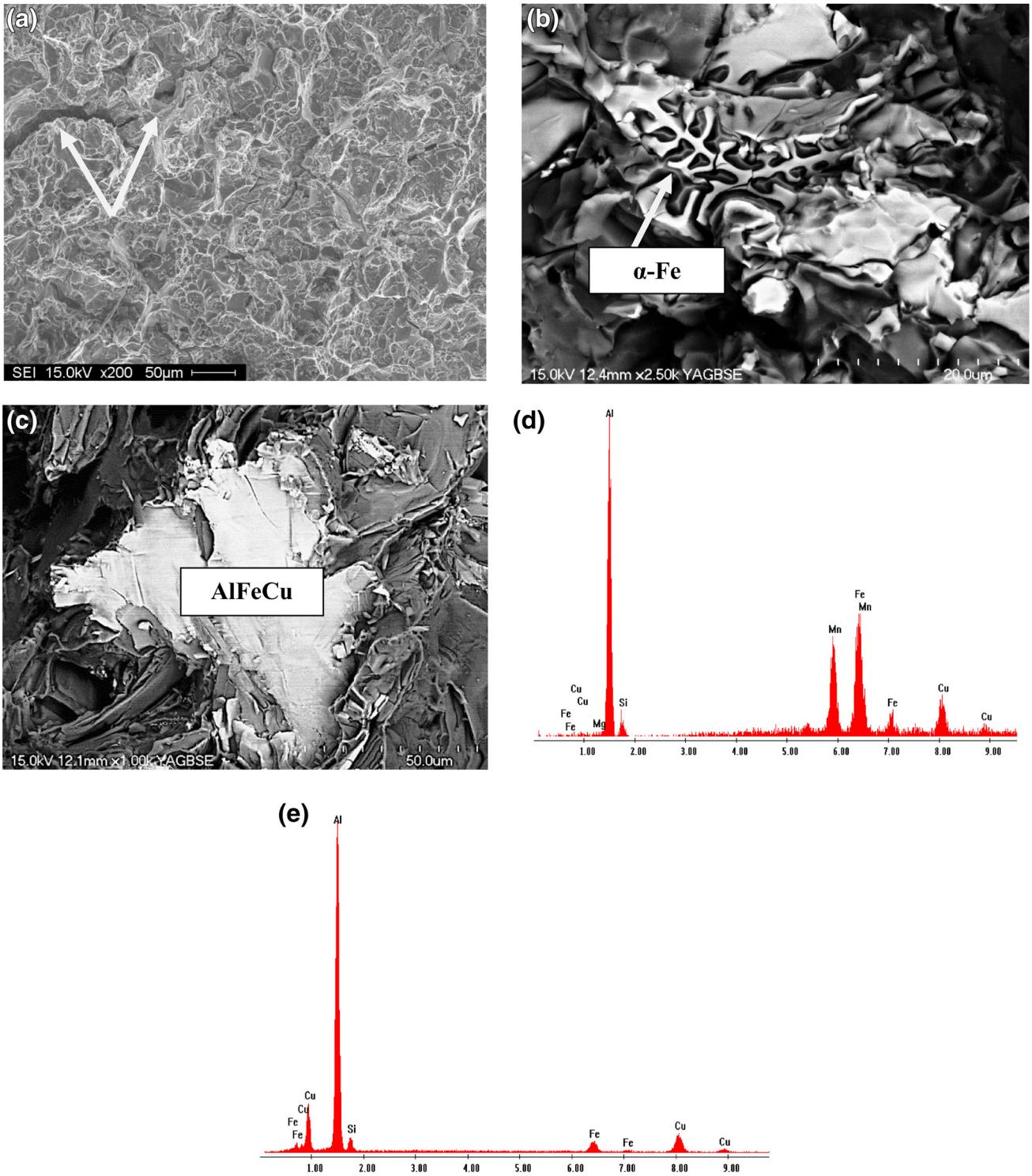

Figure 10. Graphics show a series of electron images and EDSs taken from the newly developed alloy following the new aging regime: (a) general view showing the presence of several cracks; (b) high-magnification image revealing the presence of α-Fe phase; (c) high-magnification image exhibiting the fracture of undissolved AlFeCu phase; (d) EDS spectrum corresponding to (b); and (e) EDS spectrum corresponding to (c).

Fractography

Figure 9a presents the fracture surface of the newly developed alloy after the homogenization treatment. Large deep dimples can be seen throughout the surface with broken particles at their interiors. The corresponding EDS spectrum, Figure 9b, reveals that these particles are mainly Fe-based intermetallic phases. The surface fracture of the aged new alloy (with UTS approximately 1GPa), Figure 10a, exhibits several cracks (arrowed) along with fine dimples compared to those shown in Figure 9a. High-magnification images reveal the presence of α-Fe in its Chinese script form—Figure 10b, whereas Figure 10c shows the cleavage fracture of undissolved AlFeCu phase particles. Figure 10d, e show the EDS spectra corresponding to Figure 10b, c, respectively.

Conclusions

Based on the results obtained from our investigation of the means to increase the strength of 7075-type wrought alloys through adjustments in alloy chemistry and heat treatment conditions, the following conclusions may be drawn.

1. Solution heat treatment for 48 h at 460 °C (860 °F) and 470 °C (878 °F) results in dissolution of Mg-rich and Cu- rich phases, whereas Fe-rich phases remain in the matrix.
2. With the use of proper additives, cold/hot deformation, homogenization and aging, as applied in this study, 7075 alloys have the potential to reach UTS levels as high as 850 MPa after aging (compared to 580 MPa obtained from traditional 7075 alloy).
3. Alloy ductility may be significantly improved using proper casting technology. It is expected that the modification of both alloy composition and casting technique will provide higher percentage elongation values.
4. The observed marked increase in the alloy strength by adjusting the alloy chemistry and heat treatment may be attributed to precipitation of dense ultrafine particles of Al_2Cu phase distributed uniformly throughout the matrix.
5. With proper composition and heat/thermomechanical treatment, it is expected that the alloy can achieve an ultimate tensile strength of about 1 GPa with about 5 % elongation.

Acknowledgments

The authors would like to thank Dr. Ehab Samuel of NRC-ATC (Quebec, Canada) for reviewing the present article.

REFERENCES

1. I.J. Polmear, Recent developments in light alloys. Mater. Trans., JIM **37**(1), 12–31 (1996)
2. H.Y. Hunsicker, Development of Al–Zn–Mg–Cu alloys for aircraft, in *Proceedings Rosenhain Century Conference* (Metals Society, London, 1976), pp. 359–376
3. J.T. Staley, History of wrought–aluminium–alloy development, in *Aluminium Alloys: Contemporary Research and Applications, Treaties on Materials Science and Technology*, vol. 31 (Academic Press, London, 1989), pp. 3–31
4. Patent No. EP0377779B2, in *Aluminum Alloy Product Having Improved Combinations of Strength, Toughness and Corrosion Resistance*. New European Patent Specification, Bulletin 2001/36, (5 September 2001)
5. N.E. Paton, A.W. Sommer, Influence of thermomechanical processing treatments on properties of aluminum alloys, in *Proceedings of Third International Conference on Strength of Metals and Alloys*, vol. 1 (Metals Society, London, 1973), pp. 101–108
6. A. Yamamoto et al., Calorimetric and resistivity study of formation and redissolution of precipitates in 7050 aluminum alloy. Mater. Trans., JIM **39**(1), 69–74 (1998)
7. S.K. Panigrahi, R. Jayaganthan, Development of ultrafine grained high strength age hardenable Al 7075 alloy by cryorolling. Mater. Des. **32**, 3150–3160 (2011)
8. A. Joshi, C.R. Shastry, M. Levy, Effect of heat treatment on solute concentration at grain boundaries in 7075 aluminum alloy. Metall. Trans. A **12A**, 1081–1088 (1981)
9. M.E. Fine, Precipitation hardening of aluminum alloys. Metall. Trans. A **6A**, 625–630 (1975)
10. J.K. Park, A.J. Ardell, Microstructures of the commercial 7075 Al alloy in the T651 and T7 tempers. Metall. Trans. A **14A**, 1957–1965 (1983)
11. A. Karaaslan, I. Kaya, H. Atapek, Effect of aging temperature and of retrogression treatment time on the microstructure and mechanical properties of alloy AA 7075. Met. Sci. Heat Treat. **49**(9–10), 443–447 (2007)
12. J.K. Park, A.J. Ardell, Effect of retrogression and re-aging treatments on the microstructure of Al-7075-T651. Metall. Trans. A **15A**, 1531–1543 (1984)
13. S.V. Emani et al., Double aging and thermomechanical heat treatment of AA 7075 aluminum alloy extrusions. J. Mater. Sci. **44**, 6384–6391 (2009)
14. R.N. Lumley, I.J. Polmear, A.J. Morton, Temper developments using secondary aging. Mater. Forum **28**, 85–95 (2004)
15. G.A. Farhadi, A.M. Samuel, F.H. Samuel, B. Kulunk, Parameters controlling the performance of Al–Si–Mg automotive alloys containing Fe-intermetallics: Part

Ii—work hardening behavior, in *Proceedings International Symposium on Light Metals*, COM 2001, August 26–29, Toronto, ON, Canada, pp. 323–338 (2001)
16. G. Farhadi, A.M. Samuel, F.H. Samuel, B. Kulunk, Effect of Trace elements and heat treatment on the microstructure and performance of 6XXX Aluminum automotive skin: part II alloy formability. Alum. Trans. **4–5**, 17–24 (2001)
17. G.A. Farhadi, A.M. Samuel, F.H. Samuel, H.W. Doty, B. Kulunk, Alloy performance in relation to intermetallic fragmentation observed in 5XXX aluminum alloys in the Sr-modified and annealed conditions, in *International Symposium on Light Metals*, Ottawa, ON, Canada, August 20–23, pp. 71–93 (2000)
18. M.F. Ibrahim, A.M. Samuel, F.H. Samuel, A preliminary study on optimizing the heat treatment of high strength Al–Cu–Mg–Zn alloys. Mater. Des. **57**, 342–350 (2014)
19. A. Nabawy, A.M. Samuel, F.H. Samuel, H.W. Doty, Influence of additions of Zr, Ti–B, Sr, and Si as well as of mold temperature on the hot-tearing susceptibility of an experimental Al–2% Cu–1% Si alloy. J. Mater. Sci. **47**, 4146–4158 (2012)
20. J.T. Staley, R.H. Brown, R. Schmidt, Heat treating characteristics of high strength Al–Zn–Mg–Cu alloys with and without silver additions. Metall. Trans. **3**, 191–199 (1972)
21. O.N. Senkov et al., Microstructure and properties of cast ingots of Al–Zn–Mg–Cu alloys modified with Sc and Zr. Metall. Mater. Trans. A **36A**, 2115–2126 (2005)
22. Y.L. Wu et al., Microalloying of Sc, Ni, and Ce in an advanced Al–Zn–Mg–Cu alloy. Metall. Mater. Trans. A **30A**, 1017–1024 (1999)
23. M. Alipour, M. Emamy, Effects of Al–5Ti–1B on the structure and hardness of a super high strength aluminum alloy produced by strain-induced melt activation process. Mater. Des. **32**, 4485–4492 (2011)